THE UCSD RADIO-SELECTED QUASAR SURVEY FOR DAMPED Lyα SYSTEMS

REGINA A. JORGENSON,[1] ARTHUR M. WOLFE,[1] JASON X. PROCHASKA,[2] LIMIN LU,[3] J. CHRISTOPHER HOWK,[4]
JEFF COOKE,[1,5] ERIC GAWISER,[6] AND DAWN M. GELINO[7]

ABSTRACT

As large optical quasar surveys for DLAs become a reality and the study of star-forming gas in the early universe achieves statistical robustness, it is now vital to identify and quantify the sources of systematic error. Because the nature of optically selected quasar surveys makes them vulnerable to dust obscuration, we have undertaken a radio-selected quasar survey for DLAs to address this bias. We present the definition and results of this survey. We then combine our sample with the CORALS data set to investigate the H I column density distribution function $f_{H\,I}(N, X)$ of DLAs toward radio-selected quasars. We find that $f_{H\,I}(N, X)$ is well fitted by a power law $f_{H\,I}(N, X) = k_1 N^{\alpha_1}$, with $\log k_1 = 22.90$ and $\alpha_1 = -2.18^{+0.20}_{-0.26}$. This power law is in excellent agreement with that of optically selected samples at low $N_{H\,I}$, an important yet expected result given that obscuration should have negligible effect at these gas columns. However, because of the relatively small size of the radio-selected sample, 26 DLAs in 119 quasars, $f_{H\,I}(N, X)$ is not well constrained at large $N_{H\,I}$, and the first moment of the H I distribution function, Ω_g, is, strictly speaking, a lower limit. The power law is steep enough, however, that extrapolating it to higher column densities implies only a modest, logarithmic increase in Ω_g. The radio-selected value of $\Omega_g = 1.15^{+0.37}_{-0.38} \times 10^{-3}$ agrees well with the results of optically selected surveys. While our results indicate that dust obscuration is likely not a major issue for surveys of DLAs, we estimate that a radio-selected sample of $\approx$100 DLAs will be required to obtain the precision necessary to absolutely confirm an absence of dust bias.

Subject headings: galaxies: evolution — intergalactic medium — quasars: absorption lines

Online material: color figures

1. INTRODUCTION

The introduction of large data sets from surveys such as the Sloan Digital Sky Survey (SDSS) has made possible statistically significant studies of damped Lyα systems (DLAs; Prochaska et al. 2005, hereafter PHW05), quasar absorption systems defined as having an H I column density $N_{H\,I} \geq 2 \times 10^{20}$ cm^{-2} and that contain most of the neutral gas in the redshift interval $z = [0, 5]$ (Wolfe et al. 2005). These large surveys for DLAs shed light on the history of the neutral gas content of the universe and show how it is affected by star formation and gas replenishment. However, one major problem consistently affects magnitude-limited optical surveys: the issue of intervening dust and the possibility of obscuration bias. Because the metallicities of DLAs can be as high as one-third solar and are always above 1/1000 solar (Prochaska 2003), the presence of dust in these objects is not surprising. Specifically, evidence from element abundance patterns suggests the presence of depletion (Pettini et al. 1999), while evidence for differential reddening suggests that dust obscuration is possible (Pei & Fall 1995). Dust obscuration in optically selected surveys could be introducing a selection bias against DLAs whose high dust optical depth would hide the background quasar. This effect could seriously impact the results of statistics and derived values such as Ω_g, the cosmological density of neutral gas (see Pei & Fall 1995), particularly since high column density systems that dominate Ω_g would be theoretically most likely to have strong obscuration. Here and throughout the paper we use Ω_g to mean Ω_g^{DLA}, the neutral gas contained in systems defined as being DLAs, i.e., with an H I surface density $N_{H\,I} \geq 2 \times 10^{20}$ cm^{-2}. For a detailed discussion of the rationale behind this choice, see PHW05.

Because radio observations are insensitive to the presence of dust, a radio-selected sample of quasars does not suffer from this dust obscuration selection effect. Therefore, a radio-selected survey is a check on the possible introduction of biases in the magnitude-limited, optical surveys. One previous survey, the Complete Optical and Radio Absorption Line System (CORALS) survey by Ellison et al. (2001), attempted to answer the question of the importance of dust obscuration by selecting quasars from the Parkes quarter-Jansky Flat-spectrum Radio Survey (Jackson et al. 2002) and then following up with optical observations of the selected quasars, regardless of magnitude, to search for the presence of DLAs. Ellison et al. found a slightly higher incidence of DLAs than that found by optical surveys. From their measurement of Ω_g, Ellison et al. concluded that the effects of dust could be suppressing the magnitude-limited value of Ω_g by no more than a factor of 2.

The radio-selected surveys were motivated by several studies that indicated that dust obscuration would significantly bias the results of Ω_g and other quantities derived from optical surveys. Fall & Pei (1993) constructed models to predict the possibility of dust obscuration of quasars and found that between 10% and 70% of quasars at $z = 3$ could be obscured, resulting in an underestimate of Ω_g by the optical surveys. Recently, Wild & Hewett (2005) reported on a survey of SDSS quasars for Ca II

[1] Department of Physics, and Center for Astrophysics and Space Sciences, University of California at San Diego, 9500 Gilman Drive, La Jolla, CA 92093-0424; regina@physics.ucsd.edu, awolfe@ucsd.edu.

[2] Department of Astronomy and Astrophysics, UCO/Lick Observatory, University of California, 1156 High Street, Santa Cruz, CA 95064; xavier@ucolick.org.

[3] Lucent Technologies, P.O. Box 3033, Naperville, IL 60566-7033.

[4] Department of Physics, University of Notre Dame, 225 Nieuwland Science Hall, Notre Dame, IN 46556.

[5] Center for Cosmology, University of California at Irvine, Irvine CA 92697-4575; cooke@uci.edu.

[6] NSF Astronomy and Astrophysics Postdoctoral Fellow; Astronomy Department and Center for Astronomy and Astrophysics, Yale University P.O. Box 208101, New Haven, CT 06520-8101.

[7] Michelson Science Center, California Institute of Technology, MS 100-22, 770 South Wilson Avenue, Pasadena, CA 91125.

absorption-line systems with $0.84 < z_{abs} < 1.3$. Using Ca II along with Fe and Mg lines; they claimed that most of their sample likely contains DLAs and a significant amount of reddening. By modeling the reddening of these systems they made an estimate that they were missing $\approx 40\%$ of Ca II systems from the SDSS due to dust obscuration, which they compared favorably to the upper limit of the CORALS survey.

On the other hand, the SDSS-DR3 survey that found 525 DLAs (PHW05) indicates that a dust bias, if present, is not an important effect. Prochaska et al. examined their results as a function of quasar magnitude, separating out the brightest 33% and the faintest 33% of the sample in each of four redshift bins. While there is not a statistically significant difference in the line density, they measured 40% higher Ω_g values toward brighter quasars at the 95% confidence level (c.l.). Since this is the opposite effect of what the dust bias would naively imply (a dust bias may imply that $\Omega_g^{bright} < \Omega_g^{faint}$, since the brightest observed quasars should have less foreground dust obscuration, which implies a smaller $N_{H I}$ value and hence smaller Ω_g), the SDSS-DR3 results with a statistically significant higher value of Ω_g toward brighter quasars point to the conclusion that dust obscuration is not an important effect. When Murphy & Liske (2004) examined the results of the SDSS-DR2, a sample including 70 DLAs, they found no evidence for reddening. After examining the much larger SDSS-DR3, M. T. Murphy et al. (2005, private communication) found evidence for reddening, but at a very low level—the implied dust-to-gas ratio is less than 0.02, where the dust-to-gas ratio is defined relative to that of the Milky Way (see eq. [7] of Wolfe et al. [2003]). However, with all of these studies it is important to remember that optical samples cannot measure dust bias in objects so heavily extincted that they are missing from the samples. As larger optical surveys for DLAs become feasible, due to surveys such as the SDSS, and the statistical uncertainties become <5%, potential causes of systematic uncertainties, such as dust obscuration, must be fully understood.

In this paper we present the results of a radio-selected quasar survey that was undertaken by our group. This UCSD sample is approximately the same size as the CORALS sample and presents a comparable assessment of dust obscuration. We analyze the combined results, attempt to assess the H I column density distribution function, $f_{H I}(N, X)$, and show that our results for Ω_g do not differ in a statistically significant way from the results of optically selected surveys, therefore suggesting that dust obscuration is most likely not a major problem affecting optically selected quasar samples for DLAs.

The organization of this paper is as follows. In § 2 we describe the UCSD quasar sample, DLA identification method, and analysis processes. In § 3 we review the standard DLA statistical analysis methods. We discuss the results of the UCSD, CORALS, and combined samples in § 4, as well our process for dealing with the empty fields. And finally, in § 5 we compare our results with the most recent optical surveys.

Throughout the paper we use the following cosmological parameters (Bennett et al. 2003): $\Omega_\Lambda = 0.7$, $\Omega_m = 0.3$, $H_0 = 70$ km s^{-1} Mpc^{-1}.

2. THE UCSD SAMPLE

The UCSD sample consists of 68 objects selected from the 411 sources that comprise the complete Caltech-Jodrell Bank radio catalogs, including the Pearson-Readhead sample (PR), the Caltech-Jodrell Bank VLBI Surveys 1 and 2 (CJ1 and CJ2), and the Caltech-Jodrell Bank Flat-spectrum sample (CJF) completion. While each sample was selected by a progressively lower

TABLE 1
DETAILS OF OBSERVATIONS

Telescope	Date (Number of Nights)	Resolution (at 4000 Å)	Number of Quasars Observed
Palomar	1995 Nov (2)	4–6	17
Palomar	1996 Apr (1)	4–6	8
Palomar	1996 May (2)	4–6	9
Palomar	1996 Dec (2)	4–6	16
Palomar	1997 Jun (1)	4–6	7
Keck LRIS	2001 Nov (1)	4–6	3
Keck ESI..........	2002 Apr (1)	0.5	14
Keck ESI..........	2002 Aug (1)	0.5	7
Keck LRIS	2002 Dec (1)	11	1
Keck LRIS	2003 May (1)	3–5	14

flux density threshold, the sources for each sample were all selected to have declination (B1950.0) $\delta \geq 35°$ and Galactic latitude $|b| \geq 10°$. The PR sample includes 65 objects with flux density at 6 cm (4859 MHz), $S_{6 cm} \geq 1.3$ Jy (Pearson & Readhead 1988). The CJ1 sample includes 135 sources with flux density at 6 cm, 1.3 Jy $\geq S_{6 cm} \geq 0.7$ Jy (Polatidis et al. 1995; Thakkar et al. 1995; Xu et al. 1995), and the CJ2 sample consists of 193 mostly flat-spectrum objects with a flux density $S_{6 cm} \geq 350$ mJy (Taylor et al. 1994; Henstock et al. 1995). The CJF (Taylor et al. 1996) is a compilation of the flat-spectrum radio sources (spectral index flatter than $\alpha_{1400 MHz}^{4850 MHz} \geq -0.5$) from the previous three surveys, plus and additional 18 sources for completion.

An optical campaign to determine the type of source, magnitude, and redshift of the radio catalog objects followed, the results of which were compiled in the CJ catalogs. The object optical identification and determination of the R magnitude was done by automated scanning of the POSS plates or by eye. Redshifts were primarily taken from Veron-Cetty & Veron (1993) and Henstock et al. (1997).

From this large radio sample, our selection criterion included all objects identified as quasars with $z_{em} > 2.0$ regardless of optical magnitude. The $z_{em} > 2.0$ cutoff was chosen to ensure sufficient spectral coverage to search for DLAs at wavelengths redward of the atmospheric cutoff at ≈ 3200 Å. We also included in our sample of 68 objects all 14 sources designated as optical EFs in order to be sure that we were not artificially selecting objects brighter than an arbitrary optical magnitude. And finally, we included the five sources for which there was a tentative optical identification, but no redshift information.

2.1. Observations and Analysis

Observations of most quasar candidate objects were first carried out at Palomar, with follow-up done at Keck for faint or "empty field" (EF) objects (see Table 1). The majority of our spectra have better than 6 Å FWHM. Five of the 68 objects in our sample were previously observed at moderate spectral resolution, and the data or results for these objects were taken from the literature. These included quasars Q0014+813, Q0201+365, Q0636+680, and Q0642+449, which were observed by Sargent et al. (1989), and quasar Q1124+571, which was taken from Lanzetta et al. (1991). The $N_{H I}$ measurement for the DLA toward Q0201+365 was taken from Lu et al. (1993).

Initial observations of most other targets were made with the 200 inch Hale telescope of the Palomar Observatory. Observations were made with the Double Spectrograph and used gratings that were 300 lines mm^{-1} in the blue and the 315 lines mm^{-1} in the red, resulting in 4–6 Å resolution using the 1″ slit, and ≈ 10 Å

TABLE 2
UCSD Survey Sample

Quasar	z_{em}	R mag	$N_{H\,I} \times 10^{20}$ cm^{-2}	z_{abs}	z_{min}	z_{max}	6 cm Flux (Jy)	Survey[a]
Q0014+813	3.384	15.9	...	...	1.591	3.340	0.551	CJ2
Q0153+744	2.338	16.0	...	...	1.568	2.305	1.794	PR
Q0201+365	2.912	17.5	2.4[b]	2.461	1.632	2.873	0.349	CJ2
Q0212+735	2.367	19.0	...	...	1.742	2.333	2.444	PR
Q0604+728	3.53	20.3	...	...	2.651	3.485	0.654	CJ2
Q0609+607	2.710	19.0	...	...	1.650	2.673	1.059	CJ2
Q0620+389	3.470	20.0	...	...	1.842	3.425	0.87	CJ1
Q0627+532	2.200	18.5	...	...	1.619	2.168	0.485	CJ2
Q0636+680	3.174	16.2	...	...	1.591	3.132	0.499	CJ2
Q0642+449	3.406	18.5	...	...	1.591	3.362	0.78	CJ1
Q0727+409	2.501	17.0	...	...	1.578	2.466	0.468	CJ2
Q0738+491	2.318	21.0	...	...	1.928	2.285	0.352	CJ2
Q0749+426	3.590	18.1	...	...	2.118	3.544	0.461	CJ2
Q0800+618	3.04	19.6	3.16 ± 0.15	2.9603 ± 0.0017	2.234	3.000	0.981	CJ2
Q0803+452	2.102	19.6	...	...	1.594	2.071	0.414	CJ2
Q0824+355	2.249	19.7	2.0[c]	2.2433	1.655	2.217	0.746	CJ2
Q0833+585	2.101	18.0	...	...	1.546	2.070	1.11	CJ1
Q0836+710	2.180	16.5	...	...	1.507	2.148	2.423	PR
Q0902+490	2.690	17.2	...	...	1.550	2.653	0.547	CJ2
Q0917+449	2.180	19.0	...	...	1.578	2.148	0.80	CJ1
Q0930+493	2.590	18.4	...	...	1.666	2.554	0.574	CJ2
Q1014+615	2.800	18.1	2.5[c]	2.7670	2.263	2.757	0.631	CJ2
Q1053+704	2.492	18.5	...	...	1.801	2.457	0.71	CJ1
Q1124+571	2.890	18.0	...	...	1.796	2.851	0.597	CJ2
Q1144+542	2.201	20.5	...	...	1.632	2.169	0.88	CJ1
Q1155+486	2.028	19.9	...	...	1.632	1.998	0.445	CJ2
Q1214+588	2.547	19.5	...	...	1.632	2.512	0.307	CJ2
Q1239+376	3.818	19.5	2.0 ± 0.15	3.4082[d]	2.344	3.770	0.446	CJ2
Q1325+436	2.073	18.5	...	...	1.549	2.042	0.533	CJ2
Q1333+459	2.449	18.5	...	...	1.612	2.414	0.76	CJ1
Q1337+637	2.558	18.5	...	...	1.550	2.522	0.431	CJ2
Q1413+373	2.360	17.3	...	...	1.607	2.326	0.383	CJ2
Q1421+482	2.220	18.9	...	...	1.549	2.188	0.536	CJ2
Q1427+543	2.980	20.7	...	...	2.331	2.940	0.718	CJ2
Q1435+638	2.068	15.0	...	...	1.591	2.037	1.24	CJ1
Q1526+670	3.020	17.1	...	...	1.977	2.980	0.417	CJ2
Q1547+507	2.169	18.5	...	...	1.582	2.137	0.74	CJ1
Q1602+576	2.858	16.8	...	...	1.630	2.819	0.351	CJ2
Q1624+416	2.550	22.0	...	...	1.732	2.515	1.632	PR
Q1645+635	2.380	19.4	3.55 ± 0.15	2.1253 ± 0.0003	1.536	2.346	0.444	CJ2
Q1745+624	3.886	18.3	...	...	3.085	3.837	0.580	CJ2
Q1755+578	2.110	18.6	25.1 ± 0.15	1.9698 ± 0.0009	1.630	2.079	0.455	CJ2
Q1758+388	2.092	17.8	...	...	1.512	2.061	0.92	CJ1
Q1834+612	2.274	17.6	...	...	1.599	2.241	0.590	CJ2
Q1839+389	3.094	19.5	5.0 ± 0.15	2.7746 ± 0.0009	1.911	3.053	0.476	CJ2
Q1850+402	2.120	17.9	20.0 ± 0.25	1.9888 ± 0.0058	1.669	2.089	0.535	CJ2
Q2015+657	2.845	19.1	...	...	2.734	2.807	0.500	CJ2
Q2017+745	2.187	17.9	...	...	1.602	2.155	0.500	CJ2
Q2136+824	2.350	18.9	...	...	2.002	2.317	0.509	CJ2
Q2255+416	2.150	20.9	...	...	2.119	2.119	0.99	CJ1
Q2259+371	2.228	20.4	...	...	1.632	2.196	0.406	CJ2
Q2310+385	2.181	17.5	...	...	1.630	2.149	0.484	CJ2
Q2356+385	2.704	18.6	...	...	1.771	2.666	0.449	CJ2

[a] CJ1, CJ2 = Caltech Jodrell Bank; PR = Pearson-Readhead.
[b] $N_{H\,I}$ value taken from Lu et al. (1993).
[c] Associated systems: z_{abs} within $\approx$3000 km s^{-1} of z_{em}.
[d] Weak metals; therefore, best fit is determined by eye.

resolution using the 2″ slit when conditions were poor. All data were reduced using standard IRAF reduction packages.

Follow-up observations of EFs and faint quasars were done at Keck with the Echellette Spectrograph and Imager (ESI; Sheinis et al. 2002) and the Low Resolution Imaging Spectrometer (LRIS;

Oke et al. 1995). With LRIS, the slit size was generally 0″.7. The ESI observations used the 1″.0 slit in LowD mode and the 0″.5 slit in echellette mode.

Fifteen of the original 68 objects were excluded from the final statistical data set for the following reasons: seven were determined

TABLE 3
EMPTY OR EXTENDED FIELDS

Object	R.A. (J2000.0)	Decl. (J2000.0)	Exposure Time (s)	$R_{\lim}$ 3 σ[a]	Morphology (arcsec)	R mag[b]	6 cm Flux (Jy)	Survey
0102+480	01 05 49.93	+48 19 03.19	294	26.1	No detection	...	1.080	CJ1
0633+596	06 38 02.87	+59 33 22.21	500	26.4	Possibly extended	25.8 ± 0.7	0.482	CJ2
0718+793	07 26 11.74	+79 11 31.0	500	26.1	Extended, $\approx 7 \times 3$	24.5 ± 0.4	0.467[c]	CJ2
1107+607	11 10 13.09	+60 28 42.57	600	26.5	Extended, $\approx 4 \times 2.5$	25.8 ± 0.8	0.400	CJ2
1205+544	12 08 27.50	+54 13 19.53	600	26.5	Possibly extended	24.6 ± 0.3	0.397	CJ2
1312+533	13 14 43.83	+53 06 27.73	600	26.5	Extended, $\approx 3 \times 3$	25.4 ± 0.6	0.433	CJ2
1828+399	18 29 56.52	+39 57 34.69	900	26.9	No detection	...	0.353	CJ2
2054+611[d]	20 55 38.84	+61 22 00.64	900	26.7	Possibly extended	...	0.414	CJ2

NOTE.—Units of right ascension are hours, minutes, and seconds, and units of declination are degrees, arcminutes, and arcseconds.
[a] Limiting magnitude per seeing element above sky background.
[b] R magnitude estimation of extended smudge.
[c] At 1.4 GHz.
[d] Uncertain identification: either $z = 1.588$, 3.0, or 3.3.

to be galaxies, stars, or low-redshift quasars, and the remaining eight were deemed EFs. Table 2 contains the details of the final 53 quasars used in the UCSD statistics, while Table 3 and Table 4 contain a summary of the EFs and the discarded objects, respectively.

2.2. Damped Lyα Systems

The Palomar data were reduced using standard IRAF packages, while the Keck data were reduced using IDL reduction software.[8] The reduced quasar spectra were continuum fitted and normalized and then analyzed to find regions in which the rest-frame equivalent width of an absorption feature was ≥ 5 Å and located in a region of good signal-to-noise ratio (S/N). The equivalent width of the spectrum was calculated, and an equivalent width array was then analyzed for regions that were greater than the 5 Å rest-frame cutoff, as explained by Wolfe et al. (1995). We searched all regions of the spectrum blueward of Lyα emission, beginning with the lowest wavelength at which the error was below the rest-frame equivalent width threshold of ≥ 5 Å at the 5 σ level. All candidate detections were then inspected by eye to determine if they were indeed DLAs. False detections were usually quite obvious to exclude as blended lines, Lyβ, etc.

Nine DLAs were found, two of which, toward quasars Q0824+355 and Q1014+615, were within 3000 km s^{-1} of the Lyα emission peak, and therefore considered "associated." Following the standard practice, we exclude these associated DLAs from the sample in order to ensure that we are not detecting objects that are physically associated with the quasar. Discarding

these two leaves a final seven DLAs to be included in the UCSD sample.

2.2.1. Lyα Fits

The DLA systems were fitted with Voigt profiles using the IDL tool[9] x_fitdla, which allows the user to interactively modify the Voigt profile and continuum placement. In all but one case, that of Q1239+376, the DLA redshift was constrained by the corresponding metal lines with errors as given in Table 2. In the case of Q1239+376, the metal lines were too weak for use in constraining the DLA redshift, and we instead determined the best fit interactively by eye using x_fitdla. This method results in larger uncertainties for z_{abs} and $N_{H\,I}$.

For most of our sample DLAs a conservative estimate of the uncertainty in $N_{H\,I}$ is 0.15 dex. However, in one case, that of Q1850+402, where the Voigt profile proved difficult to fit, we report an uncertainty of 0.25 dex in $N_{H\,I}$. Figure 1 shows Voigt profile fits for each DLA, except for the $z_{abs} = 2.461$ DLA toward Q0201+365, which is in the existing literature (Sargent et al. 1989). Now we give brief details on each DLA system.

Q0201+365.—$N_{H\,I}$ fit taken from Lu et al. (1993) and discussion therein.

Q0800+618.—The difficulty in estimating the continuum placement in such close proximity to the Lyα emission peak made this DLA system somewhat difficult to fit. There is also a possibility of some blended absorption.

Q1239+376.—High S/N and good placement. The only problem with this fit was some blending on the red side.

Q1645+635.—High S/N and lack of blending resulted in a good Voigt profile fit to this DLA profile.

Q1755+578.—Close proximity to Lyα emission peak and blending on the blueward side made the fit difficult.

Q1839+389.—Straightforward fit and good continuum.

Q1850+402.—Close proximity to Lyα emission peak, lower S/N and blending made this a more difficult fit, yielding an increased error margin on the Voigt profile of 0.25 dex.

[8] See http://www.ucolick.org/∼xavier/IDL.

TABLE 4
DISCARDED OBJECTS

Object	Reason for Discard	Survey
0843+575	Galaxy	CJ2
1125+596	Quasar at $z_{em} = 1.78$	CJ2
1308+471	Galaxy	CJ2
1436+763	Star	CJ2
1809+568	No significant emission feature	CJ2
2238+410	Spectrum dubious	CJ2
2319+444	Quasar at $z_{em} = 1.24$	CJ2

3. DLA STATISTICS

Our goal of determining the impact of dust obscuration in surveys of DLAs requires that we be able to compare our radio-selected survey to the results of optically selected surveys. We
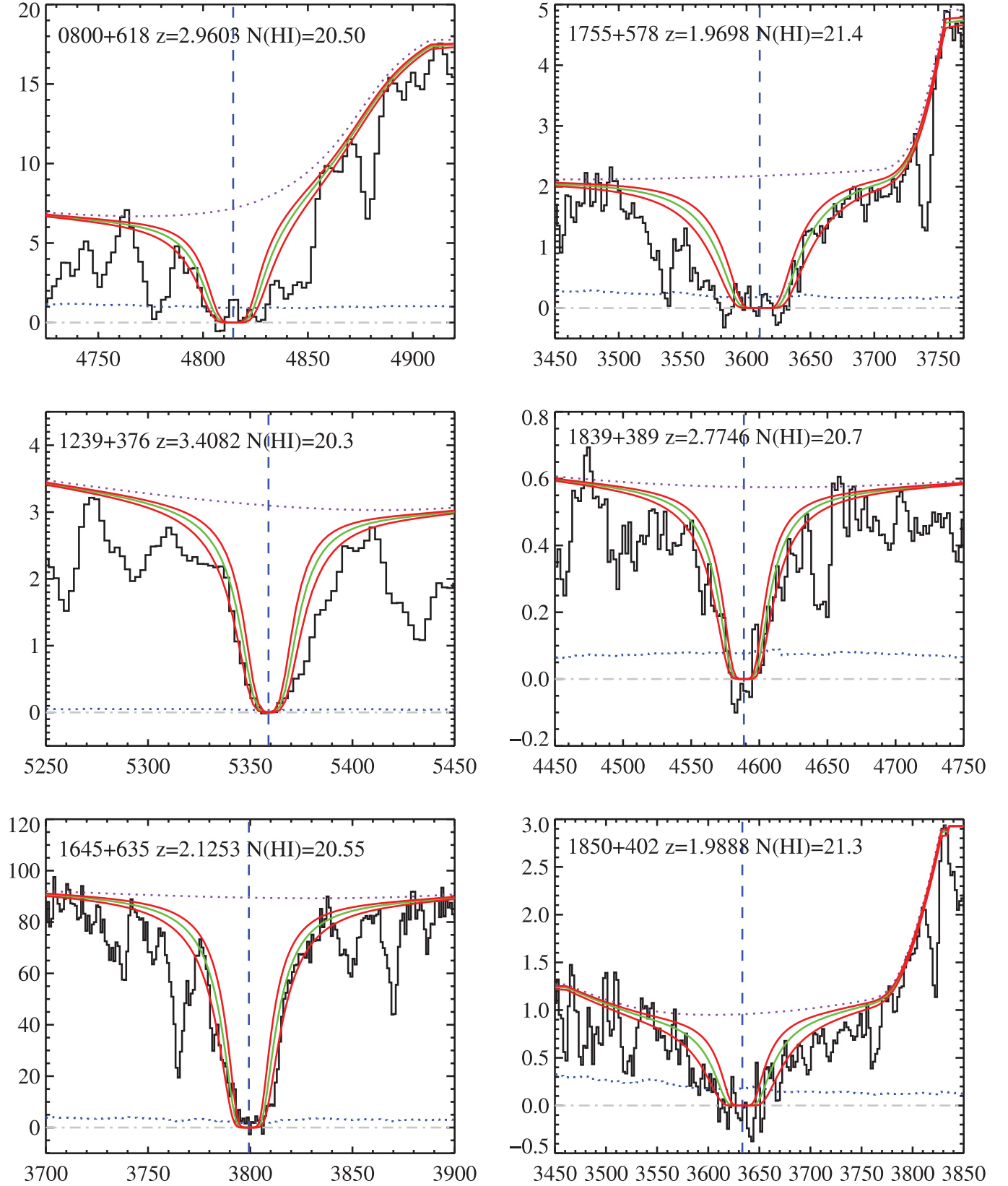
[9] See http://www.ucolick.org/∼xavier/IDL.

Fig. 1.—Voigt profile DLA fits for the six new DLA systems in the UCSD sample. The best Voigt profile is indicated by the green curve, surrounded by profiles with $N_{\rm H\,I}$ displacements ± 0.15 dex (or ± 0.25 dex) in red. The continuum placement can be seen as the purple dotted line, while the error array is represented by the blue dotted line.

now introduce some of the standard statistical quantities used to describe and quantify surveys of DLAs.

3.1. Δz, $g(z)$, and $n(z)$

The redshift path, Δz, is defined as the total redshift interval along which a damped Lyα feature with rest-frame equivalent width exceeding 5 Å would be detected at more than 5 σ significance. It is defined as

$$\Delta z = \sum_{i=1}^{n} \left(z_i^{\max} - z_i^{\min} \right), \tag{1}$$

where the summation is over the n quasars in the survey, $z_{\min}$ is determined to be the lowest spectral wavelength with good S/N, and $z_{\max}$ is the redshift corresponding to the maximum spectral wavelength included in the search. We define $z_{\max}$ by

$$z_{\max} \equiv z_{\rm qso} - (1 + z_{\rm qso})/100. \tag{2}$$

This corresponds to 3000 km s^{-1} blueward of the Lyα emission feature. This cutoff ensures that a damped Lyα system is not physically associated with the quasar.

The redshift path density, $g(z)$, gives an idea of the statistical significance as a function of redshift of a survey for DLAs. It is defined as the number of quasars with sight lines containing a particular redshift interval (Lanzetta et al. 1991). Specifically,

$$g(z) = \sum_{i=1}^{n} H \left(z_i^{\max} - z \right) H \left(z - z_i^{\min} \right), \tag{3}$$

where H is the Heaviside step function, the sum is over n quasars (Lanzetta et al. 1991), and

$$\Delta z = \int g(z) \, dz, \tag{4}$$

where the integral is over all z paths in the survey. The DLA number density, $n(z)$, is simply the number of DLAs per unit redshift,

$$n(z) = \frac{m}{\Delta z}, \tag{5}$$

where m is the number of DLAs.

3.2. $f_{\rm H\,I}(N, X)$: The H I Frequency Distribution Function

Following the direction of previous works such as Lanzetta et al. (1991) and PHW05, we can define a neutral hydrogen frequency distribution function that describes the number of DLAs in a range of column densities, $(N, N + dN)$, and a range of absorption distances, $(X, X + dX)$,

$$f_{\rm H\,I}(N, X) \, dN \, dX, \tag{6}$$

where the absorption distance, ΔX, is defined as

$$\Delta X = \int dX \equiv \int \frac{H_0}{H(z)} \, (1 + z)^2 \, dz, \tag{7}$$

where H_0 is the Hubble constant.

3.3. $\ell_{\rm DLA}(X)$: The Damped Lyα Line Density

The zeroth moment of the H I frequency distribution function is known as the line density of DLAs, $\ell_{\rm DLA}(X)$. The line density

represents the number of systems per unit absorption distance and is defined as

$$\ell_{\rm DLA}(X) = \int_{N_t}^{\infty} f_{\rm H\,I}(N, X) \, dN. \tag{8}$$

As described in PHW05, the line density is related to the covering fraction of DLAs on the sky. This relationship is apparent if we describe the frequency distribution function in terms of an average cross section $A(X)$, and the comoving number density of DLAs, $n_{\rm DLA}(X)$:

$$f_{\rm H\,I}(N, X) \equiv (c/H_0) n_{\rm DLA}(X) A(X) \tag{9}$$

(see Wolfe et al. [2005] for details).

3.4. Ω_g: The Cosmological Neutral Gas Mass Density

An important parameter in describing any quasar survey for DLAs is the first moment of the H I frequency distribution function, the neutral gas mass density, Ω_g. It is believed that Ω_g is closely related to the amount of neutral hydrogen available for star formation and, hence, places an important tracer on the history of star formation in the universe. Acquiring this parameter through surveys for DLAs is an important constraint on the neutral gas reservoir available for star formation in the early ($z > 2$) universe; Ω_g is defined as

$$\Omega_g(X) \equiv \frac{\mu m_{\rm H} H_0}{c \rho_c} \int_{N_{\min}}^{N_{\max}} N f_{\rm H\,I}(N, X) \, dN, \tag{10}$$

where μ is the mean molecular mass of the gas (taken to be 1.3), $m_{\rm H}$ is the mass of the hydrogen atom, ρ_c is the critical mass density, $f_{\rm H\,I}(N, X)$ is the frequency distribution function of neutral gas found in DLAs, and the integration is from $N_{\min} = 2 \times 10^{20}$ cm^{-2} to $N_{\max} = \infty$. We follow previous works (i.e., Lanzetta et al. 1991) and replace this frequency distribution function by its evaluation in the discrete limit as

$$\Omega_g = \frac{\mu m_{\rm H} H_0}{c \rho_c} \frac{\Sigma N({\rm H\,I})}{\Delta X}, \tag{11}$$

where the sum is performed over the $N_{\rm H\,I}$ measurements of the DLA systems in a given redshift interval with total path length ΔX. As emphasized by PHW05 and discussed below, equation (11) only provides an accurate evaluation of equation (10) if the survey is sufficiently large that the observed $f_{\rm H\,I}(N, X)$ distribution becomes steeper than N^{-2} at large $N_{\rm H\,I}$. If this is not the case, equation (11) provides only a lower limit to Ω_g.

4. RESULTS

We now describe the results of the UCSD radio-selected survey, the CORALS radio-selected survey, and the combination of these two surveys, which we refer to as the combined sample. Details of the results of each survey are listed in Table 5.

4.1. UCSD Survey Results

The UCSD sample consists of seven DLAs in 53 quasars of $z_{\rm em} \geq 2.0$ with a total redshift path of $\Delta z = 41.15$. This resulted in a number of DLAs per unit redshift, $n(z) = 0.17_{-0.07}^{+0.08}$, where the error bars are the standard 1 σ Poissonian errors using Gehrels' tables for small number statistics (Gehrels 1986). Figure 2 presents $g(z)$ versus z for the UCSD sample in green. The line density of DLAs over the cosmological redshift path of $\Delta X = 130.43$

TABLE 5
RESULTS

Feature	UCSD	CORALS	Combined
Number of quasars...........	53	66	119
Number of DLAs.............	7	19	26
Δz.................................	41.15	57.16	98.31
$n(z)$..................................	$0.17^{+0.08}_{-0.07}$	$0.33^{+0.10}_{-0.07}$	$0.26 \pm {}^{0.06}_{0.05}$
$\ell_{DLA}(X)$.........................	$0.05^{+0.03}_{-0.02}$	$0.10^{+0.03}_{-0.02}$	0.08 ± 0.02
$\langle N_{H\,I} \rangle$ (cm^{-2})	8.744×10^{20}	7.532×10^{20}	7.858×10^{20}
$\langle z \rangle$.................................	2.53	2.50	2.51
$\langle z \rangle_{weighted}$	2.17	2.33	2.28
$\Sigma N_{H\,I}$ (cm^{-2})	0.61×10^{22}	1.43×10^{22}	2.04×10^{22}
ΔX................................	130.43	186.68	317.11
$\Omega_g (10^{-3})$.........................	$0.84^{+0.43}_{-0.45}$	$1.37^{+0.53}_{-0.55}$	$1.15^{+0.37}_{-0.38}$
Error(%)	$\pm 54\%$	$\pm 41\%$	$\pm 33\%$

FIG. 3.—H I frequency distribution $f_{H\,I}(N, X)$ for the 26 DLAs of the combined sample in red. Overplotted are the fits of a single power law (*blue dot-dashed line*) and a Γ-function (*red dashed line*). The last bin contains the 2 σ upper limit. Plotted in black is the $f_{H\,I}(N, X)$ for the optical data from the SDSS-DR3, with the Γ-function fit in green.

resulted in $\ell_{DLA}(X) = 0.05^{+0.03}_{-0.02}$, while the mass density of neutral gas is $\Omega_g = 0.84^{+0.43}_{-0.45} \times 10^{-3}$. While we report Ω_g as a detection, it is, strictly speaking, a lower limit because we do not measure $f_{H\,I}(N, X)$ to fall off faster than N^{-2} (see § 4.3).

4.2. *CORALS Survey Results*

The CORALS survey (Ellison et al. 2001) was the first attempt to use a radio-selected quasar survey as a basis for a search for DLAs. They selected quasars from the complete Parkes quarter-Jansky flat-spectrum sample (Jackson et al. 2002), comprised of 878 radio sources with spectral index $\alpha^{5GHz}_{2.7GHz} > -0.4$ and declinations between $+2\overset{\circ}{.}5$ and $-80°$. Ellison et al. (2001) limited their data set to 66 $z_{em} \geq 2.2$ quasars in which they found 22 DLAs. Three of these DLAs were classified as associated and dropped from the final sample. Two more DLAs were excluded because they fell outside of the range $1.8 \leq z_{abs} \leq 3.5$ that Ellison et al. (2001) set for their statistical sample, citing that there appears to be little evolution of Ω_g in this range. Since the UCSD sample did not have this z^{max}_{abs} cutoff, we included all 19 CORALS DLAs in the statistics for the combined sample.

Detailed results of the CORALS survey, including the two DLAs in sight lines to quasars with $z_{abs} > 3.5$, are listed in Table 5. Statistics for the number density and neutral gas mass density in the CORALS survey resulted in their conclusion that previous, magnitude-limited surveys could have underestimated these values by as much as a factor of 2. The plot of $g(z)$ versus z for the
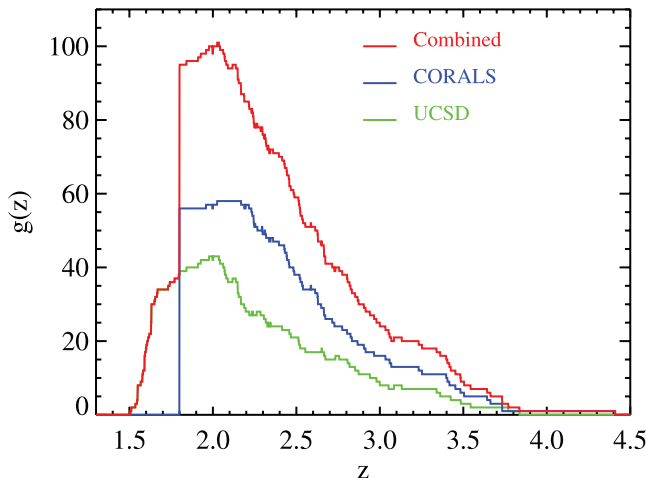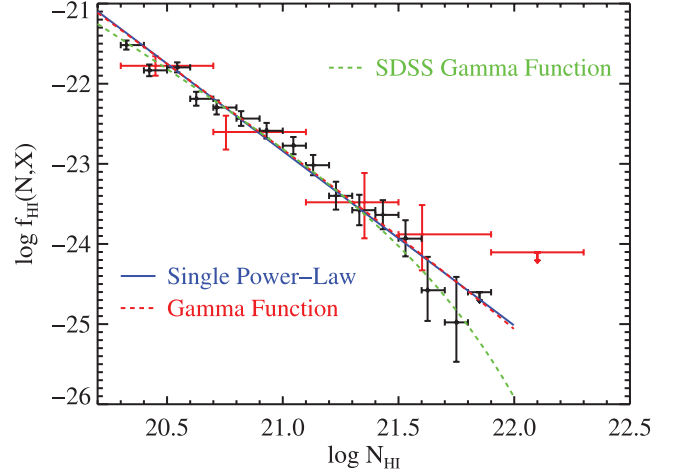
CORALS survey is shown in blue in Figure 2. Over a total redshift interval, $\Delta z = 57.16$, the number of DLAs per unit redshift, $n(z) = 0.33^{+0.10}_{-0.07}$. Over a cosmological redshift path of $\Delta X = 186.68$, the line density of DLAs in the CORALS survey, $\ell_{DLA}(X) = 0.102^{+0.03}_{-0.02}$, which is twice that of the UCSD survey. CORALS compared their neutral gas mass density in DLAs $\Omega_g = 1.37^{+0.53}_{-0.55} \times 10^{-3}$ with the compilation of Péroux et al. (2001) and Rao & Turnshek (2000), and concluded that Ω_g derived from optically selected surveys could be underestimated by up to a factor of 2.

However, Ellison et al. (2001) did concede the uncertainty of their conclusion primarily because the small survey fails to fully sample the column density distribution, and second because their high value of Ω_g is dominated by two relatively high column density systems (both incidentally in front of "moderately bright" quasars, $B = 19.5, 20$, which qualitatively matches the result of PHW05 that there is an anticorrelation between quasar magnitude and $N_{H\,I}$).

4.3. *Combined Results*

For simplicity, we present detailed analyses for just the combined sample, which has the greatest statistical significance. Figure 2 presents $g(z)$ versus z for the combined sample in red. The CORALS sample begins abruptly at $z = 1.8$, the z_{min} cutoff of their sample. The UCSD sample continues down to a $z_{min} \approx 1.51$ for some quasars. For $z \approx 2$ the combined sample is nearly twice that of CORALS. For higher redshift intervals (i.e., $z = 3$), the CORALS survey contributes roughly two-thirds of the path length. Of course, the combined sample gives the best constrained estimate of the number density of $n(z) = 0.26^{+0.06}_{-0.05}$.

The combined sample is large enough to attempt an analysis of the H I distribution function, $f_{H\,I}(N, X)$. This sample spans the redshift interval $z = [1.51, 4.4]$ with an integrated absorption path length $\Delta X = 317.11$ and a column density weighted mean redshift of 2.28. In practice, we can evaluate $f_{H\,I}(N, X)$ in the discrete limit and plot the resulting $f_{H\,I}(N, X)$ in $N_{H\,I}$ bins of some ΔN. In Figure 3 we plot in red $f_{H\,I}(N, X)$ for the combined sample, in $N_{H\,I}$ bins of $\Delta N = 0.4$ dex, calculated in the following way:

$$f_{H\,I}(N, X) = \frac{m_{DLA}(N, N + \Delta N)}{\Delta X}, \quad (12)$$

FIG. 2.—Redshift sensitivity function $g(z)$ as a function of redshift for the UCSD survey, the CORALS survey, and the combined sample.

TABLE 6

FITS TO $f_{H I}(N, X)$

Form	Parameters	SDSS-DR3 Optical Sample[a,b]	Combined Radio Sample[c]
Single	$\log k_1$	23.36	22.90
	α_1	-2.19 ± 0.05	$-2.18^{+0.20}_{-0.26}$
Gamma	$\log k_2$	-23.52 ± 0.02	$-25.97^{+0.09}_{-0.08}$
	$\log N_\gamma$	$21.48^{+0.07}_{-0.10}$	$22.49^{+0.29}_{-0.36}$
	α_2	-1.80 ± 0.06	$-2.12^{+0.22}_{-0.27}$

[a] Prochaska et al. (2005).
[b] Mean absorption redshift = 3.06.
[c] Mean absorption redshift = 2.28.

where m_{DLA} is the number of damped Lyα systems within (N, $N + \Delta N$) in the ΔX interval and the error bars are determined by Poisson uncertainty at the 84% c.l. according to the value of m_{DLA}. Also plotted, in black, are the results of the optically selected SDSS-DR3 (PHW05) survey for comparison. Following PHW05, we have overplotted the best-fit solutions of two possible functional forms of $f_{H I}(N, X)$. Because of the small sample size of this survey we attempt to fit only a single power law and a Γ-function. The single power-law form is

$$f_{H I}(N, X) = k_1 N^{\alpha_1}, \qquad (13)$$

and the Γ-function is (e.g., Fall & Pei 1993)

$$f_{H I}(N, X) = k_2 \left(\frac{N}{N_\gamma}\right)^{\alpha_2} \exp\left(\frac{-N}{N_\gamma}\right). \qquad (14)$$

We have performed a maximum likelihood analysis to constrain the parameters and set the constants k_1 and k_2. A summary of the fit parameters, along with those of the optically selected SDSS-DR3 survey for comparison, is given in Table 6. The best-fit slope of the single power law is $\alpha_1 = -2.18^{+0.20}_{-0.26}$. This single power-law slope can be compared favorably with the optical SDSS-DR3 survey single power-law slope of $\alpha_1 = -2.19 \pm 0.05$ over their entire redshift range, $z = [2.2, 5.5]$. This correspondence is expected because the radio-selected survey is dominated by the low column density end, which matches that of the optical, and can be seen as a confirmation of the two techniques.

While the single power law gives a good fit to the radio-selected data, we also attempt to fit the Γ-function for the following two reasons: first, the single power law is unphysical, i.e., the fit must turn over in order for Ω_g to converge; and second, unlike the single power law, the Γ-function provided a satisfactory fit to the optically selected data. However, unlike the optically selected sample, the radio-selected sample gives nearly the same fit for the Γ-function as for the single power law, $\alpha_2 = -2.12^{+0.22}_{-0.27}$. While we derive a formal value of the break column density $N_\gamma = 22.49^{+0.29}_{-0.36}$, we interpret this as an unrealistic extrapolation of the data. Rather, the small size of the radio-selected sample cannot reliably determine a break column density, and therefore we cannot demonstrate that our Ω_g converges.

To determine if the radio-selected data rules out the optically selected Γ-function fit, we performed a χ^2 test on the radio-selected data and optically selected Γ-function fit. The results of the χ^2 test, $\text{Prob}_1(\chi^2 > 5.96) = 1.5\%$, show that we can reject the fit at the 5% level, but not at the 1% level of confidence. While this may be evidence for modest disagreement between the two samples, we interpret this disagreement to be primarily due to the fact that we cannot constrain the radio-selected fit at
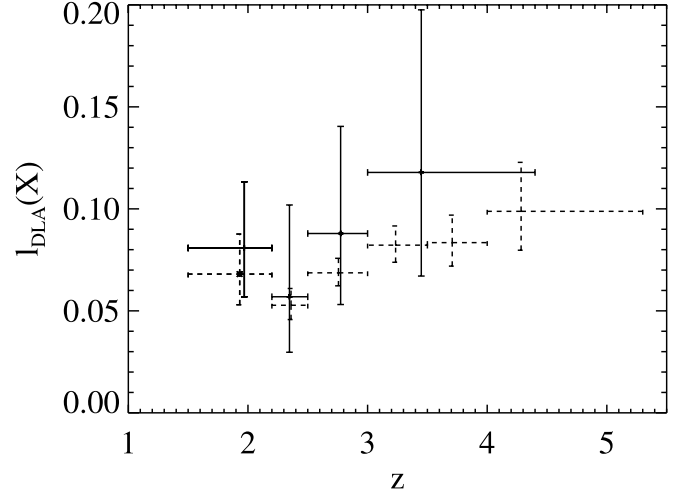

FIG. 4.—Line density of DLA systems $\ell_{DLA}(X)$ vs. redshift for the combined sample (*solid lines*). Overplotted is the $\ell_{DLA}(X)$ for the optical data from the SDSS-DR3 survey and the Péroux compilation (*dashed lines*). [*See the electronic edition of the Journal for a color version of this figure.*]

large $N_{H I}$, i.e., the radio-selected sample does not contain enough DLAs to fully sample the H I distribution function. We note that a more conservative two-sided KS test shows agreement between the radio-selected data and the optically selected Γ-function fit at the 77% level.

The line density of DLAs in the combined sample, taken over the entire redshift interval, $z = [1.5, 4.4]$, is $\ell_{DLA}(X) = 0.08 \pm 0.02$ at a median $z = 2.35$, where the errors represent the 1σ Poisson uncertainty in m_{DLA}. In Figure 4 we plot $\ell_{DLA}(X)$ for the combined sample in red, evaluated in the discrete limit,

$$\ell_{DLA}(X) = \frac{m_{DLA}}{\Delta X}. \qquad (15)$$

We have grouped the data into four redshift bins, $z = [1.5, 2.2]$, $[2.2, 2.5]$, $[2.5, 3.0]$, and $[3.0, 4.4]$, to allow for comparison with
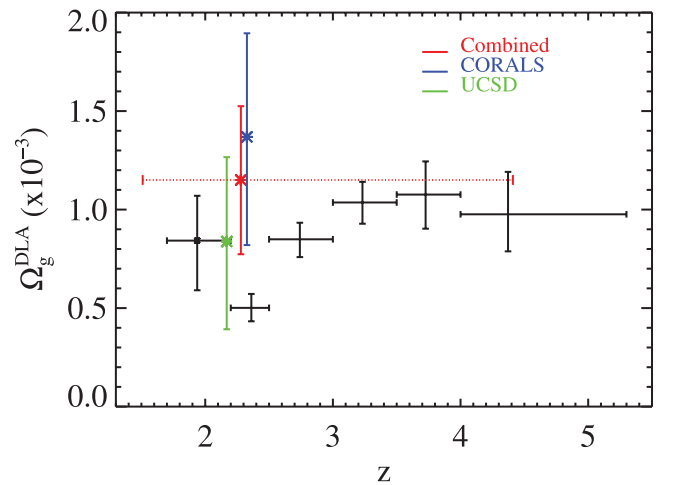

FIG. 5.—Neutral gas mass density, Ω_g, of the UCSD, CORALS, and combined samples plotted in green, blue, and red, respectively. For clarity, only the redshift bin of the combined sample is plotted, $z_{combined} = [1.51, 4.41]$ (*red dotted line*). The redshift bins of the radio samples (not plotted) are $z_{ucsd} = [1.51, 3.84]$ and $z_{corals} = [1.80, 4.41]$, and the points are plotted at the $N_{H I}$ weighted mean redshift. Also plotted are the values of Ω_g as a function of redshift for the optical SDSS-DR3 survey (*black points*). The Péroux compilation data point at $z < 2.2$ (marked with a cross) does not include measurements from the SDSS survey. All error bars are 1σ.
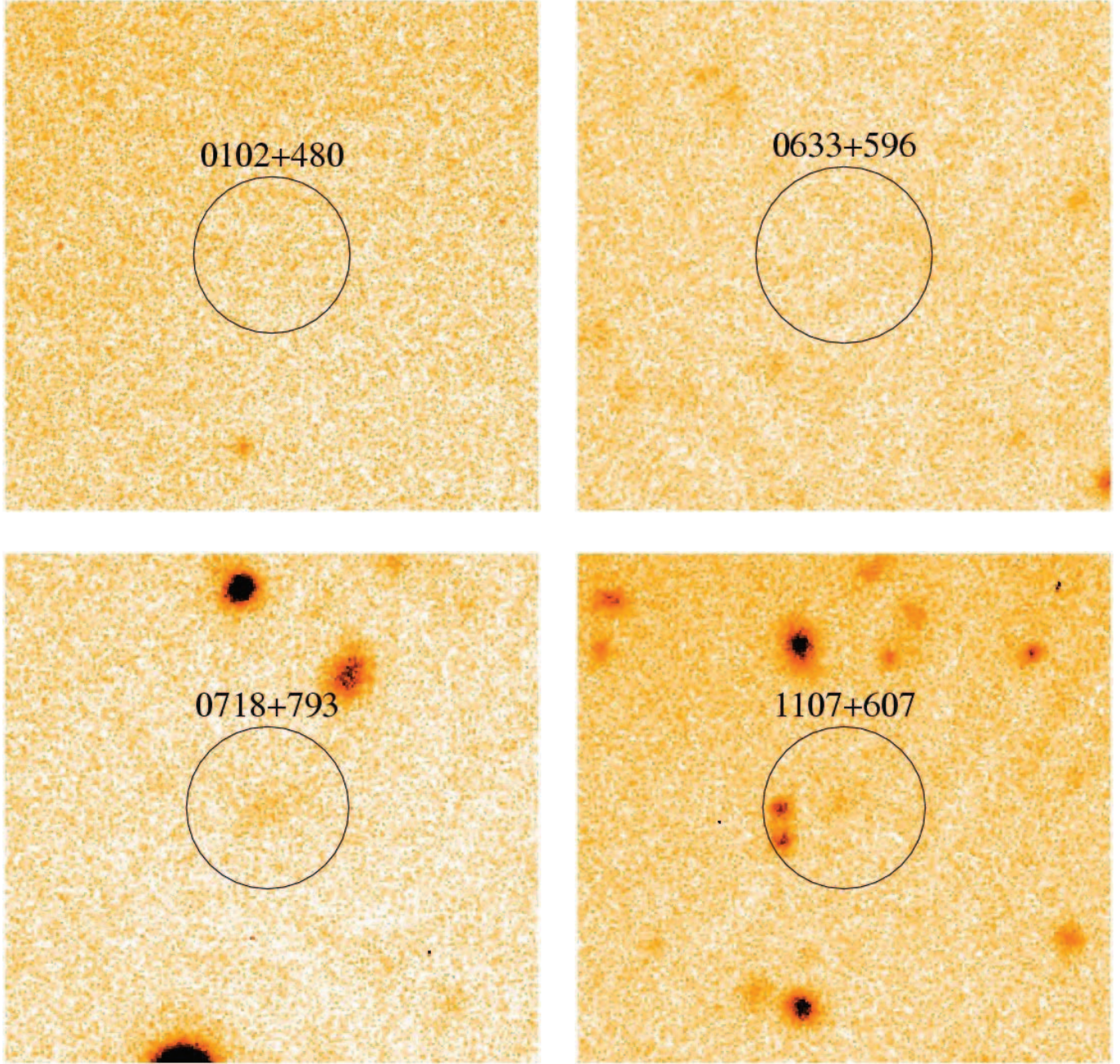
Fig. 6.—Plot of *R*-band images of the empty or extended fields. Exposure times are given in Table 3. The circle radius is $\approx 5''$. All image orientations are the standard; north is up, and east is to the left.

the results of PHW05. We have overplotted the results of the SDSS-DR3 optical survey in black. These points are grouped into redshift bins $z = [2.2, 2.5]$, $[2.5, 3.0]$, $[3.0, 3.5]$, $[3.5, 4.0]$, $[4.0, 5.3]$. The black point marked by a star in redshift bin $z = [1.5, 2.2]$ is a compilation of optical surveys for DLAs produced by Péroux et al. (2003). Although the central values of the line densities of the radio and optically selected surveys are different, the difference is not statistically significant. Note the radio sample gives a somewhat higher line density at all redshifts, and it is interesting to note that beginning at $z = 2.2$, the trend of increasing line density with increasing redshift, $z > 2.2$, is present in both samples. In fact, the central values of the radio sample follow the same qualitative shape, even the unusual "dip" at $z \approx 2.3$. While it would make sense that the SDSS-DR3 survey, with its statistically significant numbers of quasars and

DLAs, is actually detecting a physically meaningful trend— PHW05 claim the decline in $\ell_{DLA}(X)$ is due to a decrease in DLA cross section with time—the correspondence with the combined radio sample, of relatively so few objects, is likely a coincidence. However, although the error bars are large, we can interpret this similarity in line density evolution with the statistically significant results of the SDSS-DR3 as support of our results.

While we report a detection of the neutral gas mass density, $\Omega_g = 1.15^{+0.37}_{-0.38} \times 10^{-3}$, our result is actually a lower limit due to the insufficient size of the combined sample. In Figure 5 we plot Ω_g for each of the UCSD, CORALS, and combined samples. Errors are calculated using a modified bootstrap method as described by PHW05, and the values are plotted at the $N_{H\,I}$ weighted mean redshift. Also plotted, in black, are the Ω_g values determined
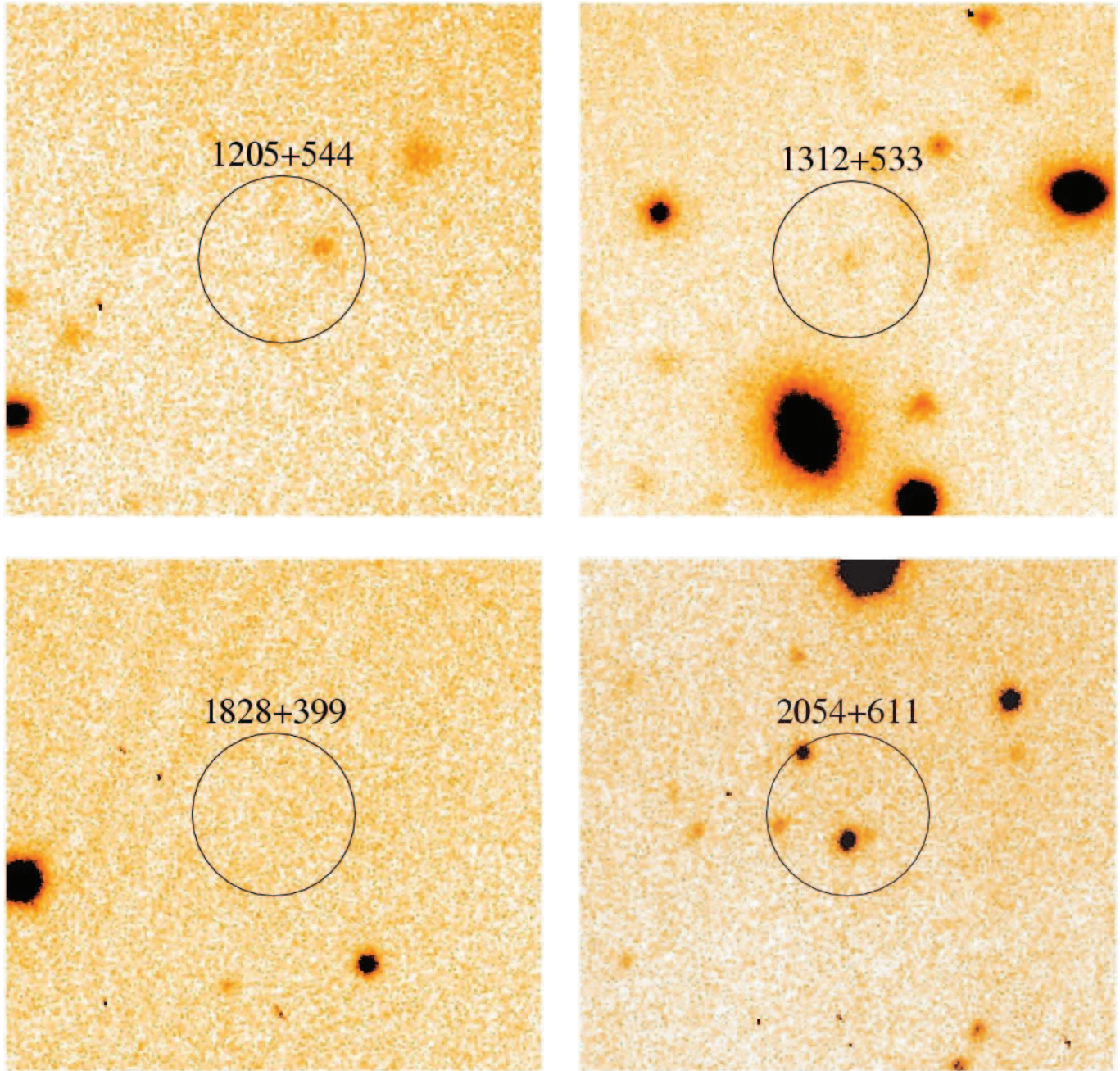
Fig. 6.—*Continued*

by the optically selected SDSS-DR3 survey (PHW05), which covers a redshift range $z \geq 2.2$. Because the SDSS-DR3 sample consists of over 500 DLAs the values of Ω_g are plotted in five redshift bins: $z = [2.2, 2.5]$, $[2.5, 3.0]$, $[3.0, 3.5]$, $[3.5, 4.0]$, and $[4.0, 5.5]$. Finally, plotted in the bin range $z = [1.7, 2.2]$, is the compilation by Péroux et al. (2003). It is seen that the lower limits of all of the radio-selected samples agree well with the optically selected data.

4.4. *Empty Fields*

The eight fields for which no optical identification of a quasar was obtained are called the empty fields (EFs). Table 3 contains the details of each EF, while Figure 6 contains Keck images of the EFs. These eight fields were determined to contain either nothing of significance, or merely a faint extended smudge when imaged with Keck in the R band for ≈ 600 s. In either case, it was not

possible to obtain spectra. While all of the previous analyses in this paper were conducted as if these fields did not exist, we actually must determine a method of including them in the sample in order for our survey to be considered complete. Assuming that the fields were truly empty, i.e., the optical source was fainter than our magnitude limit on Keck, and that pointing errors or some other experimental errors did not result in radio source misidentification, we can make two extreme, simplifying assumptions. On one hand, we can assume that no DLAs are present toward these optically faint quasars and calculate a lower limit on Ω_g by including some average redshift path length for each object, where the average path length is determined from the known quasars in our survey. On the other extreme, we can assume that each EF is actually empty because of the presence of a high column density, dusty DLA. We can assume that each EF contains an average to high column density DLA and estimate an upper limit on Ω_g.
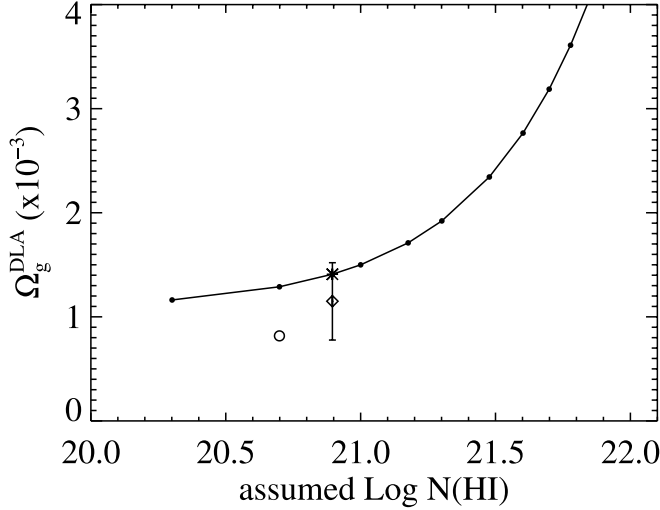
FIG. 7.—Potential impact that the EFs could have on Ω_g, the neutral gas mass density. We calculate the resulting value of Ω_g assuming that each of the eight EFs contains a DLA of the stated $N_{H\,I}$. The diamond with 1 σ error bars is the value of Ω_g found from the combined radio sample, calculated by ignoring the EFs. The asterisk represents the value of Ω_g if each of the EFs contained a DLA of our average $N_{H\,I} = 7.86 \times 10^{20}$ cm^{-2}. For reference, the optically selected SDSS survey value is plotted as an open circle. [*See the electronic edition of the Journal for a color version of this figure.*]
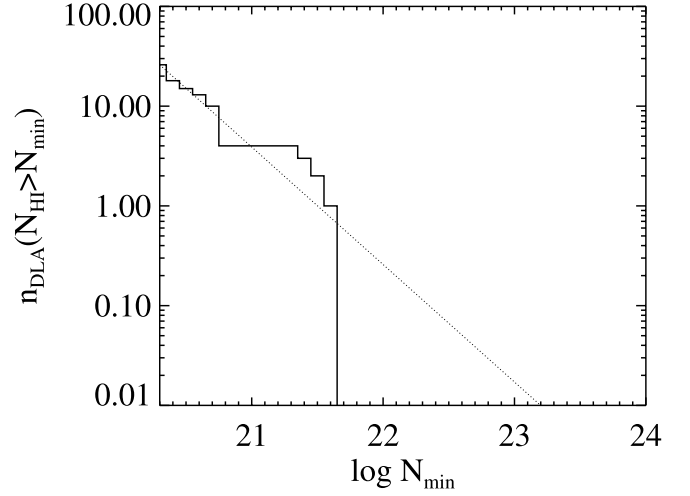

FIG. 8.—Cumulative distribution of the number of DLAs with a specific minimum $N_{H\,I}$. Overplotted is the single power-law fit to the distribution function (*dotted line*). It is seen that only 0.3 DLAs are expected with $N_{H\,I} > 10^{22}$ cm^{-2}. [*See the electronic edition of the Journal for a color version of this figure.*]

Using the results of the combined sample, we determine the average redshift path per quasar to be $\langle \Delta X \rangle = 2.66$. Assuming that each of the eight EFs would contribute this amount of redshift path gives a new total redshift path searched of $\Delta X = 338.43$. The lower limit on Ω_g, assuming that none of the EFs contained a DLA, is $\Omega_g^{lower} = 1.08 \times 10^{-3}$. The upper limit, assuming that each of the EFs contains a DLA of average column density in our survey, $N_{H\,I} = 7.86 \times 10^{20}$ cm^{-2}, results in an upper limit of $\Omega_g^{upper} = 1.41 \times 10^{-3}$. While both the lower and upper limit on Ω_g, derived by including the EFs, are clearly within the error of the combined value of $\Omega_g = 1.15^{+0.37}_{-0.38} \times 10^{-3}$, it is notable that the upper limit is only $\approx 22\%$ larger than Ω_g; i.e., even if each EF contains a dusty DLA of our average $N_{H\,I}$, the effect on Ω_g would be relatively small.

We can take the analysis one step further and allow the average value of $N_{H\,I}$ to exceed 7.86×10^{20} cm^{-2}. To determine the minimum average column density DLA that would affect our results, we assume that each EF contains a quasar at our average redshift and a DLA of fixed column density, which we vary from the lower limit, $N_{H\,I} = 2 \times 10^{20}$ cm^{-2}, to the generally observed highest column densities of $N_{H\,I} \approx 1 \times 10^{22}$ cm^{-2}. We plot the results in Figure 7.

As previously stated, if we assume that each EF contains a DLA of average column density in our survey, $N_{H\,I} = 7.86 \times 10^{20}$ cm^{-2}, we derive an $\Omega_g = 1.41 \times 10^{-3}$, indicated in Figure 7 by the asterisk. Compare this with the point and error bar, our radio-selected survey value of Ω_g, derived by ignoring the EFs. For reference, the optically selected SDSS-DR3 survey, at $\Omega_g = 0.82^{+0.05}_{-0.05} \times 10^{-3}$, is plotted as an open circle. From Figure 7 it is seen that if each EF contained a DLA of $N_{H\,I} \approx 10^{21.2}$ cm^{-2} or larger, a relatively large value occurring in only $\approx 15\%$ of our sample, the impact of the EFs would be large enough to increase the resulting value of Ω_g by $\approx 50\%$.

There are, however, several arguments for why these EFs are most likely *not* $z_{em} > 2$ quasars extinguished by very dusty, high column density DLAs. If we extrapolate the H I frequency distribution function, $f_{H\,I}(N, X)$ resulting from the radio-selected sample, as seen in Figure 3, we would expect not more than

1 DLA with $N_{H\,I} > 10^{22}$ cm^{-2}. If two or more high column density systems existed, the resulting $f_{H\,I}(N, X)$ would be unphysical assuming galaxies have declining surface density profiles. In this case, we would require a bimodal population consisting of high column density, high dust-to-gas ratio systems, such as molecular clouds, that would be missed in optical surveys.

While we cannot rule out the existence of a bimodal population, we can determine exactly how many high column density systems the current radio-selected distribution function would predict. We plot the cumulative number of DLAs above a certain minimum H I column density and extrapolate using our single power-law fit. From this plot, in Figure 8, it is apparent that we would expect only 0.3 DLAs with $N_{H\,I} > 10^{22}$ cm^{-2}. In addition, in the case of the five fields containing faint extended emission, we can use scaling arguments to show that if we assume this emission is actually the resolved quasar host galaxy, then the quasar would have to be a low-redshift object and would not have been included in our $z_{em} > 2.0$ survey. Adopting the typical high-z quasar host galaxy scale length of ≈ 12 kpc (Kuhlbrodt et al. 2005), we can estimate the angular size at $z = 2.0$ to be $\approx 1\farcs4$. Careful inspection of the extended fields reveals extended blobs of order $3''$ or larger, making these low-z quasars that would not have been included in our survey.

In an effort to determine the nature of the EFs, we are currently conducting an observing program on the Green Bank Telescope (GBT) to search for 21 cm absorption along the sight lines to these EFs. We will carry out a redshift path search from $z = [0.5, 3.9]$ using the frequencies of ≈ 300–900 MHz. If a high column density, dusty system does exist along the line of sight and is blocking out the quasar light, it is likely that we will detect it in absorption.

5. ANALYSIS AND DISCUSSION

The best way of determining the significance of dust obscuration of quasars is to compare the results of magnitude-limited and radio-selected quasar surveys for DLAs. The primary problem with this method has so far been the limited survey size of the radio-selected surveys and the resulting large error bars that preclude conclusive results. While the UCSD survey itself was slightly smaller than the previously published CORALS survey, combining the two surveys in effect doubles the size. However,
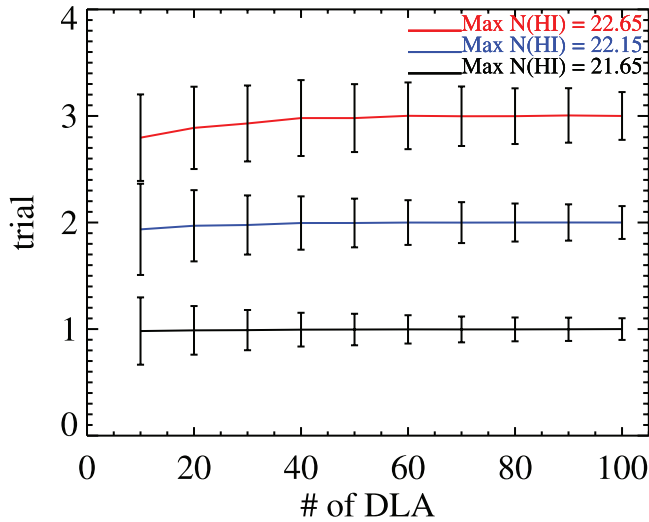
Fig. 9.—Results of bootstrapping error on samples of the given number of DLAs with maximum column densities of $N_{H\,I} = 10^{21.65}$ cm^{-2} (to match the combined sample, *black line*), $N_{H\,I} = 10^{22.15}$ cm^{-2} (*blue line*), and $N_{H\,I} = 10^{22.65}$ cm^{-2} (*red line*). It is seen that a sample with maximum $N_{H\,I} = 10^{21.65}$ cm^{-2} will give an error in the desired range of $\pm 10\%$ at ≈ 100 DLAs.

the uncertainties of the combined sample, whose size is still more than an order of magnitude smaller than the current optical samples, are so large that definitive statements remain elusive.

To make a simple estimate of the number of radio-selected DLAs necessary to conclusively answer the question of dust bias, we performed the following analysis. If we desire a result with errors of no larger than $\approx 10\%$, we can perform a bootstrap error evaluation on a random sample of DLAs, each time increasing the number of DLAs to determine how many DLAs are necessary to give the desired precision. In Figure 9 we plot the results of our bootstrap error estimation, normalized to 1 and offset for each different sample type. The estimation was performed on random $N_{H\,I}$ samples with minimum $N_{H\,I} = 10^{20.3}$ cm^{-2} and three different maximum column densities, $N_{H\,I} = 10^{21.65}$ cm^{-2}, to match the upper limit of the combined radio sample, $N_{H\,I} =$

$10^{22.15}$ and $10^{22.65}$ cm^{-2}. It can be seen that in a sample with a maximum column density similar to the combined sample, the desired $\approx 10\%$ error is achieved with a sample of ≈ 100 DLAs. As the maximum column density is increased, the error bars increase as well. Note that the bootstrap errors of our actual sample (number of DLAs = 26, error $\approx 30\%$) are slightly bigger than those of the randomly generated samples due to the fact that our sample contains only a few high column density systems.

To definitively answer the question of dust bias, we would ideally hope to at least approach the total redshift path searched by optical surveys in order to make valid comparisons. In the combined radio-selected sample, the total cosmological redshift path searched was $\Delta X = 317.11$. Compared with the total redshift path surveyed by the latest large optical survey, SDSS-DR3 with $\Delta X = 7333.2$, we are still more than an order of magnitude smaller.

The combined radio-selected central value of Ω_g is slightly higher than all of the optically selected values, as plotted in Figure 5. However, when considering the 1 σ lower limits of the radio-selected values of Ω_g, no difference between the magnitude-limited sample and the radio-selected samples can be ascertained. If we ignore the possibility of evolution in Ω_g, we can compare the entire SDSS-DR3 optically selected survey over the complete redshift range with the radio-selected value. Excluding the Péroux point, the SDSS-DR3 value taken over one redshift bin, $z = [2.2, 5.5]$, gives $\Omega_g = 0.82 \pm 0.05 \times 10^{-3}$. Comparing this value with the 1 σ lower limit of the combined radio-selected value of $\Omega_g^{low} = 0.77 \times 10^{-3}$ over the range $z = [1.51, 4.4]$, we see excellent agreement. This agreement in Ω_g between the radio and optically selected surveys for DLAs is the best evidence for our conclusion that dust bias does not have a major effect on the results of optically selected surveys.

REFERENCES

Bennett, C. L., et al. 2003, ApJS, 148, 1
Ellison, S. L., Yan, L., Hook, I. M., Pettini, M., Wall, J. V., & Shaver, P. 2001, A&A, 379, 393
Fall, S. M., & Pei, Y. C. 1993, ApJ, 402, 479
Gehrels, N. 1986, ApJ, 303, 336
Henstock, D. R., Browne, I. W. A., Wilkinson, P. N., & McMahon, R. G. 1997, MNRAS, 290, 380
Henstock, D. R., Browne, I. W. A., Wilkinson, P. N., Taylor, G. B., Vermeulen, R. C., Pearson, T. J., & Readhead, A. C. S. 1995, ApJS, 100, 1
Jackson, C. A., Wall, J. V., Shaver, P. A., Kellerman, K. I., Hook, I. M., & Hawkins, M. R. S. 2002, A&A, 386, 97
Kuhlbrodt, B., Orndahl, E., Wisotzki, L., & Jahnke, K. 2005, A&A, 439, 497
Lanzetta, K. M., Wolfe, A. M., Turnshek, D. A., Lu, L., McMahon, R. G., & Hazard, C. 1991, ApJS, 77, 1
Lu, L., Wolfe, A. M., Turnshek, D. A., & Lanzetta, K. M. 1993, ApJS, 84, 1
Murphy, M. T., & Liske, J. 2004, MNRAS, 354, L31
Oke, J. B., et al. 1995, PASP, 107, 375
Pearson, T. J., & Readhead, A. C. S. 1988, ApJ, 328, 114
Pei, Y. C., & Fall, S. M. 1995, ApJ, 454, 69
Péroux, C., McMahon, R., Storrie-Lombardi, L., & Irwin, M. J. 2003, MNRAS, 346, 1103
Péroux, C., Storrie-Lombardi, L. J., McMahon, R. G., Irwin, M., & Hook, I. M. 2001, AJ, 121, 1799

Pettini, M., Ellison, S. L., Steidel, C. C., & Bowen, D. V. 1999, ApJ, 510, 576
Polatidis, A. G., Wilkinson, P. N., Xu, W., Readhead, A. C. S., Pearson, T. J., Taylor, G. B., & Vermeulen, R. C. 1995, ApJS, 98, 1
Prochaska, J. X. 2003, in IAU Joint Discussion 15, Elemental Abundances in Old Stars and Damped Lyman-α Systems (San Francisco: ASP), 54
Prochaska, J. X., Herbert-Fort, S., & Wolfe, A. M. 2005, ApJ, 635, 123
Rao, S. M., & Turnshek, D. A. 2000, ApJS, 130, 1
Sargent, W. L. W., Steidel, C. C., & Boksenberg, A. 1989, ApJS, 69, 703
Sheinis, A. I., Bolte, M., Epps, H. W., Kibrick, R. I., Miller, J. S., Radovan, M. V., Bigelow, B. C., & Sutin, B. M. 2002, PASP, 114, 851
Taylor, G. B., Vermeulen, R. C., Readhead, A. C. S., Pearson, T. J., Henstock, D. R., & Wilkinson, P. N. 1996, ApJS, 107, 37
Taylor, G. B., et al. 1994, ApJS, 95, 345
Thakkar, D. D., Xu, W., Readhead, A. C. S., Pearson, T. J., Taylor, G. B., Vermeulen, R. C., Polatidis, A. G., & Wilkinson, P. N. 1995, ApJS, 98, 33
Veron-Cetty, M.-P., & Veron, P. 1993, A Catalogue of Quasars and Active Nuclei (Garching: ESO)
Wild, V., & Hewett, P. 2005, MNRAS, 361, L30
Wolfe, A. M., Gawiser, E., & Prochaska, J. X. 2005, ARA&A, 43, 861
Wolfe, A. M., Lanzetta, K. M., Foltz, C. B., & Chaffee, F. H. 1995, ApJ, 454, 698
Wolfe, A. M., Prochaska, J. X., & Gawiser, E. 2003, ApJ, 593, 215
Xu, W., Readhead, A. C. S., Pearson, T. J., Polatidis, A. G., & Wilkinson, P. N. 1995, ApJS, 99, 297